Recent progress of plasma exhaust concepts and divertor designs for tokamak DEMO reactors

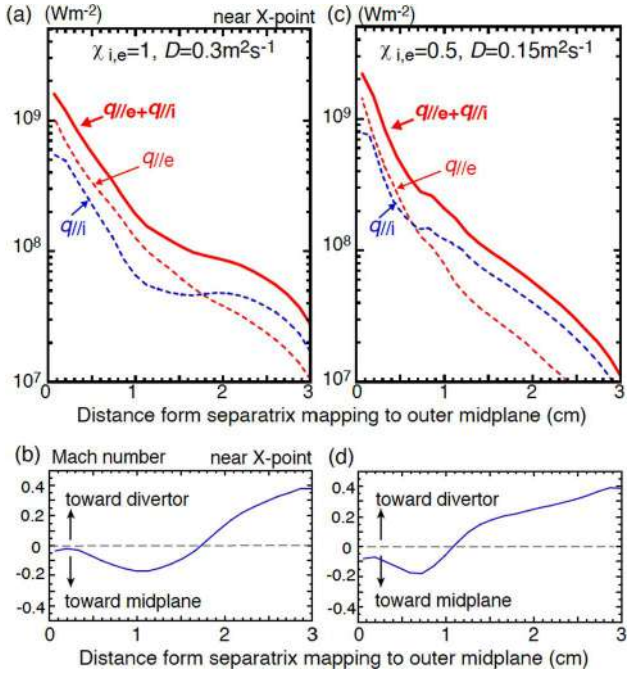

Fig. 11. Electron, ion and total parallel heat flux profiles ($q_{//e}^{Xp}$, $q_{//i}^{Xp}$, $q_{//e}^{Xp} + q_{//i}^{Xp}$) in the Low-Field-Side SOL near the X-point; (a) standard χ and D case (1.0 and 0.3 m^2s^{-1}) and (c) smaller case (0.5 and 0.15 m^2s^{-1}). Mach number profiles of the parallel plasma flow in the SOL near the X-point; (b) and (d), respectively. Minus value corresponds to the plasma flow towards the outer midplane, i.e "flow reversal". Distance from the separatrix near the X-point is mapped to the midplane SOL radius [15].

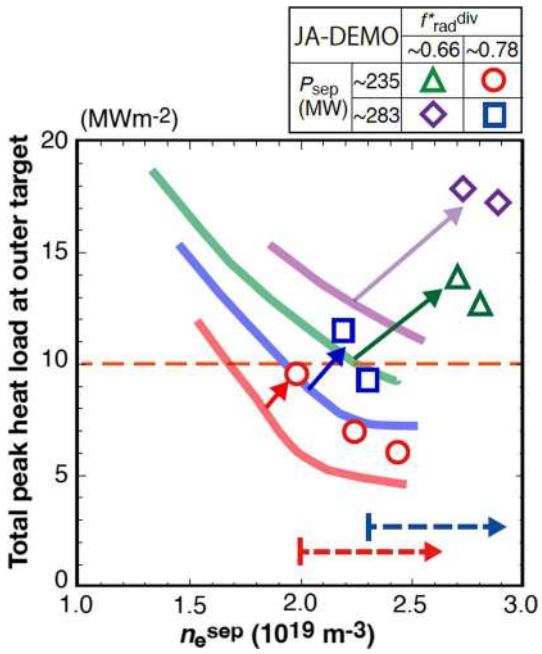

Fig. 12. Representative peak q_{target} at the outer target for four series of P_{sep} (~235/283 MW) and f_{rad}^{*div} (~0.67/0.78) as a function of n_e^{sep} [14]. Open symbols show corresponding four results with transport coefficients reduced a factor of two ($\chi_e = \chi_i = 0.5$ m^2s^{-1} and $D = 0.15$ m^2s^{-1}). Four guidelines correspond to results with standard χ and D from Fig. 6.

"far-SOL", and the former is mostly attributed by the electron conductive transport. $\lambda_{q//}^{near}$ values of $q_{//e}^{Xp}$ and $q_{//e}^{Xp} + q_{//i}^{Xp}$ profiles become smaller (from 2.3 to 1.6 mm and from 2.9 to 2.2 mm, respectively) mainly due to reduction of the radial diffusion and enhancement of the parallel conductive transport. Reference [15] (Fig. 6 (e)) showed that $\lambda_{q//}^{near}$ values of four representative $q_{//e}^{Xp} + q_{//i}^{Xp}$ profiles for the different P_{sep} and f_{rad}^{*div} cases were 1.2 – 1.6 times larger than those for the $q_{//e}^{Xp}$ profiles, and they were decreased from 2.5 – 3.3 mm (for the reference χ and D) to 1.7 – 2.2 mm for the reduced χ and D case.

On the other hand, the transition from the "near-SOL" to the "far-SOL" in the $q_{//e}^{Xp} + q_{//i}^{Xp}$ profile is attributed to the $q_{//i}^{Xp}$ profile, i.e. ion transport. Simulation results suggested that "flow reversal" [52] is produced above the outer divertor target by locally increasing neutral ionization and plasma pressure, and that it is extended to the low-field-side SOL. Fig. 11 (b) and (d) show Mach number ($V_{//}/C_s$) profiles of the plasma flow near the X-point, where the flow reversal is seen in $r^{mid} \leq$ 1.7 cm and $\leq$ 1.1 cm, respectively. The parallel convective transport is produced in the same direction. The $q_{//i}^{Xp}$ profile shows the ion heat flux towards the outer divertor, thus the convective heat flux produced by the flow reversal is not included. Flat "shoulder" in the $q_{//i}^{Xp}$ profile becomes more significant as radially extending the convective heat flux by the flow reversal, as shown in Fig. 11 (a). Since contribution of $q_{//i}^{Xp}$ on the $q_{//e}^{Xp} + q_{//i}^{Xp}$ profile becomes larger than $q_{//e}^{Xp}$ at the outer r^{mid}, the transition from the "near-SOL" to the "far-SOL" is seen outward in the $q_{//e}^{Xp} + q_{//i}^{Xp}$ profile for the standard χ and D case. Fig. 11 also shows that the transition locations of (a) $r^{mid} \sim 1.1$ cm and (c) $r^{mid} \sim 0.7$ cm correspond to peaks of the flow reversal profiles. These locations also correspond to flux surfaces of the detach-attach boundary at the outer target ($r^{div} \sim 12$ cm and ~ 7 cm, respectively). At the same time, the peak q_{target} was produced in the attached region, as shown in Reference [14] (Fig. 5), and the peak is increased from 5.8 to 9.5 MWm^{-2} mostly due to increases in the local T_e^{div} and T_i^{div}. Since the "flow reversal" reduces the impurity retention above the divertor target, the radiative cooling may not be efficient at the downstream of the flow reversal peak. These simulation results suggested that the "flow reversal" formation affects the partial detachment profile and the peak q_{target} as well as the parallel heat flux profile in SOL.

Results of the peak q_{target} at the outer target for the smaller χ and D cases are added to the results of Fig. 6, with open symbols in Fig. 12. Similar to those in Sec. 3.2, the peaks of q_{target} are increased with increasing $P_{sep}\cdot(1\text{-}f_{rad}^{*div})$ and they are reduced with increasing n_e^{sep} for each case. The lower boundary of n_e^{sep} for $q_{target} \leq 10 MWm^{-2}$ is determined to be 2.0×10^{19} and 2.3×10^{19} m^{-3} for the reference f_{rad}^{*div} (~0.78) cases: $P_{sep} = 235$ MW (red) and 283 MW (blue), respectively. Therefore, the Case-1 is acceptable in the low n_e^{sep} operation, but higher n_e^{sep} ($\geq 2.3\times10^{19}$ m^{-3}) is required for the Case-2. On the other hand, for the lower f_{rad}^{*div} (~0.67) cases, the peak q_{target} and n_e^{sep} are significantly increased with decreased partial detachment width and increased local T_e^{div} and T_i^{div}. Thus the divertor operation is difficult in the low n_e^{sep} range. As a result, the reduction in χ and D significantly affected the divertor power exhaust due to increase of the $q_{//i}$ profile in the far-SOL as well as the dominant $q_{//e}$ near the separatrix. In order to produce the detached plasma at the significantly large $q_{//}$ region and to reduce the peak $q_{target} \leq 10 MWm^{-2}$, high f_{rad}^{*div} of 0.8 level was necessary for the JA-DEMO divertor design.

4. Divertor target and heat removal design

4.1. Design concepts and key design parameters

Conceptual designs of the plasma facing components (PFCs) and coolant routing in the divertor cassette have been developed based on divertor simulation results. Since steady-state power handling of 10 MWm^{-2}-level peak heat load is a common requirement for the conventional divertor design, the water-cooled target of the ITER technology, i.e. W-monoblock (W-MB) and Cu-alloy (CuCrZr) cooling pipe [25], is a primary baseline concept. On the other hand, engineering design adequate for higher neutron irradiation condition is required for the DEMO design. Recent design concepts are summarized in Table 5;

Table 5
Key components and parameters of armor, heat sink and cassette for water-cooling divertor concepts of EU-DEMO, JA-DEMO, CFETR and K-DEMO.

		EU-DEMO [53,54]	JA-DEMO [18]	CFETR [46,55]	K-DEMO [22]
Number of cassette		48	48	80	32 (upper/lower)
Number of divertor maintenance ports		16	16	16	16
Total cassette weight incl. PFC units (ton)		8.3	~ 22	~ 8	TBD
Target	Plasma facing component	W	W	W	W
	Heat sink pipe	CuCrZr	CuCrZr	CuCrZr	CuCrZr/RAFM-steel
	Water temperature (℃)/ P(MPa)	130/ 5	200/ 5	140–180/ 5	70/4 or 290/15
	Dose rate on PFC (dpa·FPY^{-1})	< 1.9	< 0.5	< 0.5	< 0.4
	Dose rate on cooling pipe (dpa·FPY^{-1})	< 7.2	< 1.5	< 1.5	<1.9 or < 1.2
Upper target (Baffle)	Plasma facing component	(*1)	W	W	W
	Heat sink pipe	—	F82H	CuCrZr/RAFM-steel	RAFM-steel
	Water temperature (℃)/ Pressure (MPa)	—	290/ 15	140–180/ 5	150/ 5
	Dose rate on PFC (dpa·FPY^{-1})	—	< 2	< 2	< 2.6
	Dose rate on cooling pipe (dpa·FPY^{-1})	—	< 6	< 6	< 10.9
Dome (Liner)	Plasma facing component	W (*1)	W	W	W
	Heat sink pipe	EUROFER97	F82H	CuCrZr/RAFM-steel	RAFM-steel
	Water temperature (℃)/ Pressure (MPa)	180/ 3.5	290/ 15	140–180/ 5	150/ 5
	Dose rate on PFC (dpa·FPY^{-1})	< 1.8	< 1.6	< 2	< 1.9
	Dose rate on cooling pipe (dpa·FPY^{-1})	< 5	< 5	< 6	< 7.8
Cassette	Structural material	EUROFER97	F82H	SS316L/RAFM-steel	RAFM-steel
	Water temperature (℃)/ Pressure (MPa)	180/ 3.5	290/ 15	140–180/ 5	290/ 15
	Dose rate on structural material (dpa·FPY^{-1})	< 6	< 3	TBD	TBD

Note *1) Baffle is not installed. Liner is installed for protection against the plasma and neutron irradiation.

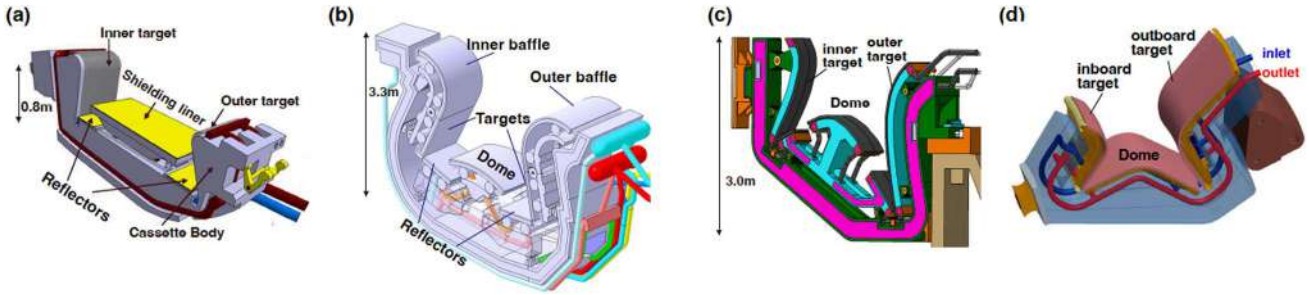

Fig. 13. Recent divertor designs for (a) EU-DEMO [54], (b) JA-DEMO [18], (c) CFETR [55], (d) K-DEMO [22].

designs of the divertor PFC units and cassette body (CB) for EU-DEMO, JA-DEMO, CFETR and K-DEMO are shown in Fig. 13. The water-cooled target concept is selected for the EU-DEMO as a baseline concept [53,54], which can take advantage of the thermal conductivity and the thermohydraulic properties compared to helium gas. All DEMO concepts have the same number (16) of the toroidal field coils (TFCs), which is less than ITER (18), and the maintenance port is located between TFCs. Three adjacent divertor cassettes are replaced through one maintenance port in both EU-DEMO (temporary option) and JA-DEMO. The divertor geometry for EU-DEMO is simplified compared to that of ITER, i.e. baffles are removed, inner and outer target plates cover ~ 0.7 m near the strike-points and a flat shielding liner is installed to protect the vaccum vessel against high neutron irradiation and to prevent gas backflow. The weight of one EU-DEMO divertor cassette is 8.3 tons, which is comparable to that of an ITER divertor cassette. JA-DEMO divertor PFC encloses most of the divertor plasma below the X-point similar to the ITER design, thus the total weight of one cassette (~22 tons) is 2.7 times heavier. In order to reduce each cassette weight for CFETR, the number of the cassettes is increased to 80.

Neutron irradiation doses, i.e. displacement per atom rate (dpa), on the W-MB and the CuCrZr heat sink are significantly increased in DEMO compared to ITER due to increasing operation time as well as the neutron flux. The maximum doses rates for a full-power-year (FPY) operation, i.e. dpa·FPY^{-1}, become larger than their doses for the full operation period of the ITER divertor, which are expected to produce 0.54 (W-MB) and 2.5 (CuCrZr) [56]. Therefore, the engineering design and technology of the divertor component should consider degradation of material properties and reductions of irradiation damage prior to the scheduled replacement. Table 5 shows that the maximum dose rates on the W-MB and CuCrZr pipe are 1.9 and 7.2 dpa·FPY^{-1}, respectively, at the upper corner of the EU-DEMO target. The former dose rate on the W-MB is comparable to those at the baffle for the other DEMO divertors, which apply the reduced activation ferritic martensitic (RAFM) steel pipe to the heat sink. It is noted that dose rates on the W-MB and CuCrZr pipe near the outer strike point for EU-DEMO are ~1 and 2 – 3 dpa·FPY^{-1}, respectively [54], both of which are larger than ~0.4 and ~1.2 dpa·FPY^{-1} for JA-DEMO [6], due to the influence of shallow divertor geometry and larger P_{fusion}.

Under severe neutron irradiation condition, reduction in thermal conductivity of the W-MB and coolant pipe, and degradation of their mechanical properties become critical issues to determine the replacement of the water-cooled divertor target in addition to various surface damages and erosion caused by the plasma irradiation as expected in ITER. For the former two factors, design issues of the PFC unit and coolant condition are explained below. Replacement of the W-MB and heat sink is prefered to be done at the same time as that of the breeding blankets (BBs) such as once in 3–4 years, which is determined by the dose restriction (such as 50 dpa) on the structual material (RAFM-steel) and the maximum dpa·FPY^{-1} on the BB for EU- and JA-DEMOs [57,58].

Reduction in the thermal conductivity of the W-MB due to the nuclear transmutation to Re and Os reaching 1 – 2 wt% at several dpa [59] will be acceptable at the high surface temperature of 500 – 1200 °C. Further factors to reduce the conductivity and mechanical properties of the armor material, i.e. bulk-W and W-alloy, by neutron irradiation and plasma surface interaction were reviewed in other references [60,61]. As shown in Sec. 3.4, net erosion by the plasma irradiation may become

a lifetime issue under the partial detached divertor condition. In addition, recrystallization will progress even at lower temperature for year-long operation such as reducing surface temperature to ~900 °C after 2.4 years [62], where the steady-state peak q_{target} may be reduced less than 10 MWm^{-2} in the later period.

Selection of Cu-alloy (CuCrZr and Cu-base composites) as the heat sink for the high heat load target is owing to their excellent thermal conductivity. On the other hand, replacement of the water-cooled target will be determined firstly by the dose on the heat sink, while the dose on the support structure (RAFM steel) is also important. Constraint factors on the material properties and their appearance doses under the neutron irradiation condition are shown in Table 6 [63]. First, radiation induced hardening at the lower temperature starts from the low irradiation dose (~0.2 dpa), then radiation induced softening and creep are anticipated at high temperarture (> 280 – 300 °C) above 1 – 2 dpa [63,64]. Therefore, degradation of the mechanical property of the Cu-alloy pipe at high temperarture with 1 – 2 dpa is anticipated as a critical lifetime issue for the high heat load PFC in JA-DEMO, K-DEMO and recent CFETR divertors, and these designs consider that it is used only for the target. For the higher dose rate (up to 5 – 6 dpa·FPY^{-1}) but lower heat load (lower than a few MWm^{-2}) region such as the baffles, reflectors and dome, the RAFM-steel pipe is applied to the heat sink. JA-DEMO anticipates replacement of the inner and outer targets after 1 – 2 year long operations, i.e. more frequently compared to the BB replacement. At the same time, the coolant temperature (T_{cool}) for the high heat flux component is increased to higher than that of ITER (~70 °C). The selection of T_{cool} has large variation between 70 °C and 200 °C at the conceptual design stage, i.e. K-DEMO: 70 °C, EU-DEMO: 130 °C, CFETR: 140 – 180 °C, JA-DEMO: 200 °C. On the other hand, for the EU-DEMO, it is tentatively assumed that the key mechanical behavior of the CuCrZr heat sink irradiated for two FPYs would not significantly change at least up to 10 dpa (reduction of thermal condictivity by transmuted product), considering the pronounced mechanical saturation behavior of CuCrZr specimens irradiated and tested at low temperature (150 °C) after a low irradiation dose (≤ 0.6 dpa) [65]. Lower T_{cool} (130 °C) for EU-DEMO is determined mainly by the requirement to ensure a safety factor of 1.4 (i.e. 40 % margin) to the critical heat flux (CHF: 45 MWm^{-2}) of the coolant for the slow-transient high heat load of 20 MWm^{-2} with 10 s. Additional discussions of the coolant condition are described in Sec. 4.2.2 and 4.2.3. A comprehensive database of these properties, design criteria and their improvement are required to determine the life time of the power handling unit.

4.2. *Design status and issues of heat removal components, cassette and coolant condition*

Design of the plasma facing component (PFC) for the 10 MWm^{-2}-level peak heat load, arrangement of coolant routing and selection of the coolant condition have been investigated for the different DEMO divertor concepts. Design status is shortly reviewed, and common design issues are clarified below.

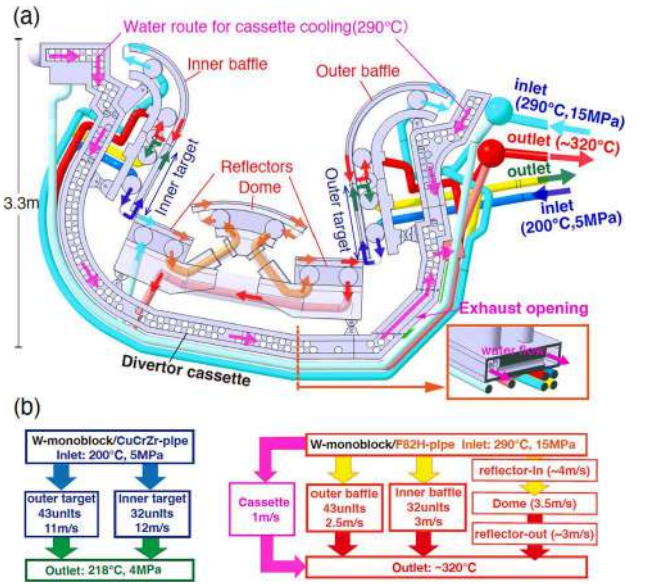

Fig. 14. Design of JA- DEMO divertor (2020): (a) arrangement of the targets, baffles, reflectors, dome and cooling pipes in a cassette, (b) flow velocity (inlet), coolant temperature and pressure in the CuCrZr and F82H pipes for the heat sink units. Here, heat removal is evaluated assuming both the inner and outer q_{target} to be 10 MWm^{-2}, which was larger than the simulation result in Sec. 3.2. [18].

4.2.1. *High heat flux PFC and coolant route design*

The arrangements of the JA-DEMO divertor and the coolant routes are shown in Fig. 14 (a) and (b). The W-MB and CuCrZr pipe PFC units cover the high heat load region of 0.8 m near the inner and outer strike-points. The coolant route for the two targets is recently revised to be parallel circuit [18] in order to supply the coolant with the velocity (V_{cool}) of 14 – 16 $m{\cdot}s^{-1}$ in the swirled pipe. This reduces the pressure drop to be less than 1 MPa at the inner target incorporating a smaller number of W-MB units, i.e. 32 and 43 for the inner and outer units. In addition, corrosion on the inner wall of the pipe above 200 °C is a common design issue. Corrosion of the inner target pipe by the high T_{cool} and V_{cool} coolant will be reduced.

The divertor configuration and coolant routing for the EU-DEMO have been revised to the one shown in Fig. 15 (a-c) [54]. The length of the vertical target (VT) of ~0.7 m is comparable to the JA-DEMO divertor target (~0.8 m). The parallel circuit concept is also a baseline of the EU-DEMO divertor. The coolant route is divided to the inner and outer targets (incorporating 32 and 44 W-MB units, respectively), and V_{cool} is comparable for both targets (14 – 16 $m{\cdot}s^{-1}$ in swirled cooling pipe). The parallel circuit design for the high heat flux PFCs becomes a common design for the two DEMO divertors, while the series circuit is used for the ITER divertor.

The W-MB and F82H pipe unit is used in the higher neutron irradiation region of the JA-DEMO divertor such as the dome, reflectors and

Table 6
Design constrains of Cu and Cu-alloy under neutron irradiation condition [63].

	Softening				Embrittlement	Thermal cond.reduction
Heat sink/ Coolant pipe	Yield strength at RT (MPa)	Threshold (℃)	Radiation-induced (dpa)		Embrittlement by transmuted He (dpa)	Reduction (20%) by transmuted product (dpa)
			hardening	softening		
Cu	~ 60 MPa	—	~ 0.1	—	6 (at 350℃) 40 appm limit with	10
CuCrZr	> 400 MPa	280	~ 0.2	~ 1	7appm/dpa	10
ODS-Cu(GlidCop® [63])	> 400 MPa	300	~ 0.2	1 ~ 2		10

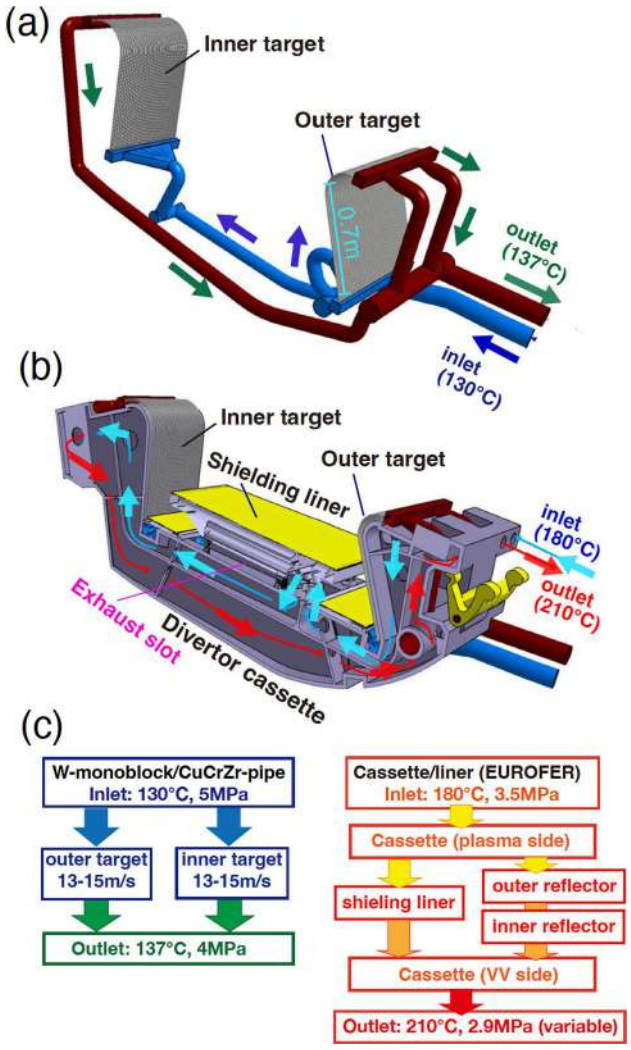

Fig. 15. Recent design of EU-DEMO divertor (2019) [54]: (a) cassette with target plates, shielding liner and cooling manifold with higher temperature (180–210 °C) coolant route shown by arrows. (b) Arrows show lower temperature (130–140 °C) coolant route for inner and outer targets. (c) Flow velocity, coolant temperature, pressure for targets and cassette body.

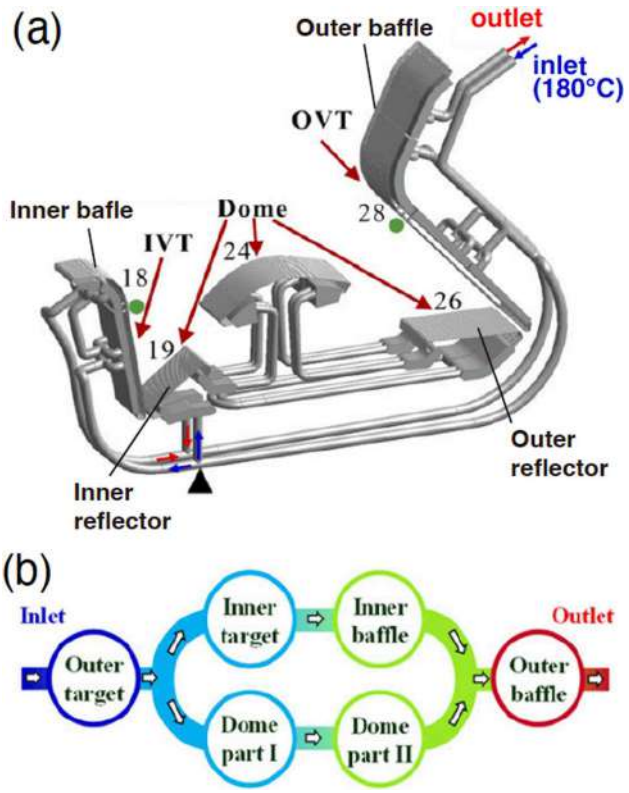

Fig. 16. (a) Hybrid coolant circuit concept for CFETR divertor [55]; OVT: outer target and baffle; IVT: inner target and baffle; Dome: umbrella, inner and outer reflector plates. The number labels show the quantity of the cooling unit channels. (b) Schematic of streaming sequence of the coolant. Dome part I and II describe Dome module divided toroidally.

baffles. Higher T_{cool} and pressurized water (290 °C, 15 MPa) similar to the BB design [67] is used for the electricity generation by turbine system similar to a pressurized water fission reactor (PWR). The maximum heat load to the W-MB surface is 1 – 1.5 MWm^{-2} and V_{cool} is relatively small (3 – 4 $m{\cdot}s^{-1}$) in the steady-state operation. Thus, the coolant route to the dome and reflectors is arranged by a series connection due to reducing the route branches and joints as shown in Fig. 14 (b). On the other hand, it is revised to the parallel one to exhaust the nuclear heat on the support structures as well as the PFC units.

The divertor configuration and water routing for the CFETR were recently improved. The divertor design and coolant routing was developed from a simple parallel one [46] to a hybrid one [55] as shown in Fig. 13 (c) and 16 (a), respectively. The divertor consists of three plasma facing modules (inner target, dome and outer target) and the CB, and all components are cooled by single coolant condition. The former design proposed that reflector plates and baffle were connected to the target module, where the CuCrZr pipe is used for all target and dome modules. Low T_{cool} (140 °C, 5 MPa) coolant was provided in parallel to inlets of the three modules in order to provide similar flow velocity of 10 $m{\cdot}s^{-1}$ to the inner and outer targets since the in-out asymmetry of the W-MB unit numbers (18 and 28, respectively) is larger than those for EU- and JA-DEMO divertors. A hybrid routing is proposed to improve the heat removal of the outer target more efficiently, and to apply the W-MB units with RAFM-steel pipes at baffles and dome similar to the JA-DEMO divertor. Therefore, T_{cool} is increased to 180 °C comparable to the CB coolant for the EU-DEMO divertor. The flow scheme is shown in Fig. 16 (b). In the hybrid circuit, the main coolant flow is provided to the inner vertical target (IVT), then divided to the inner target and baffle route and to the dome one in parallel. The two routes are merged into the outer baffle. Here, the dome circuit is separated toroidally to two half structures (Dome part I and II), and the coolant circulates through the inner reflector, dome and outer reflector of the Dome part I, then it is returned in the Dome part II. The mass flow rates for IVT and Dome routes are 12.2 and 7.1 $kg{\cdot}s^{-1}$, respectively. The pressure drop for the two routes is similar (0.79 MPa), but the total one from the OVT to the outer baffle is increased to 1.95 MPa.

Finally, the K-DEMO divertor consists of simply three plasma facing modules (inner target, dome and outer target) and the CB as shown in Fig. 13 (d) [22]. The dome structure is low height and extends to the inner and outer reflectors. While the coolant routing is not proposed, thermal analysis on the W-MB units with CuCrZr and RAFM-steel pipes is performed under the steady-state peak heat load of 10 MWm^{-2} [68]. The W-MB size with the CuCrZr pipe is comparable to that of ITER and that with RAFM-steel pipe is smaller, and the coolant conditions correspond to 70 °C/4 MPa and 290 °C/15 MPa, respectively. The former shows a similar result to the ITER divertor target, i.e. the maximum temperatures of the W-MB and CuCrZr pipe are ~ 1242 °C and ~ 271 °C, respectively. On the other hand, for the latter case, the maximum temperature reaches a softening boundary of the RAFM-steel (~550 °C) at the pipe top surface even though the pipe thickness is very thin (0.25 mm). Design of the W-MB units and coolant routing is in progress.

4.2.2. Coolant and Cu-alloy pipe temperatures for high heat flux PFC

For the JA-DEMO divertor design, the total thermal power to the PFC surface is assumed to be 325 MW, which includes about 40 % margin above the simulation result (P_{sep} ~ 235 MW), and the total volumetric nuclear heating in the PFCs and the cassette body by neutron and γ-ray fluxes (114 MW) is considered [18]. Total thermal power to the inner and outer target components is dominant compared to the nuclear heat, and the thermal powers to the dome, baffles and reflectors are still larger by the factor of 1.5 – 3. Temperature distribution on the fish-scale surface W-MB and CuCrZr pipe are evaluated under high plasma heat load (peak q_{target} of ~10 MWm^{-2}) and nuclear heating conditions. Since relatively high T_{cool} (200 °C) coolant is provided in order to minimize the irradiation embrittlement, the maximum temperatures of W-MB and CuCrZr pipe correspond to, respectively, ~1190 °C (W-MB), which is just below the critical temperature of W-recrystallization (~1200 °C), and ~350 °C (CuCrZr pipe), where the influence of thermal softening is somehow accommodated above ~300 °C [66].

For the EU-DEMO divertor design, the total thermal power to the PFC surface (targets, shielding liner and reflection plates) is given to be 200 MW, which is 33% above the simulation value of P_{sep} ~ 150 MW, and the total volumetric nuclear heat in the PFC units and the CB is 139 MW [54]. The total thermal power is smaller than that of the JA-DEMO divertor design due to smaller P_{sep} and design margin, and the nuclear heat is larger due to larger P_{fusion}. For the local coolant temperature of 150 °C near the strike point, the maximum temperatures of the CuCrZr pipe are evaluated to be ~310 °C and ~440 °C at the upper location near the strike point for the peak q_{target} of 10 and 20 MWm^{-2}-level, respectively, corresponding to the steady-state and slow transient cases. The former is slightly higher than the optimal temperature range of 250 – 300 °C, and the latter is expected to cause a reduction in the yield strength, in particular, under the neutron irradiation. Inlet T_{cool} is recently reduced from 150 to 130 °C in order to increase the CHF to larger than 45 MWm^{-2} as shown in Table 5.

As a result, the lower T_{cool} design is preferable from the viewpoints of the influence of thermal softening even for the maximum steady-state heat load (~10 MWm^{-2}) for the DEMO divertor design. On the other hand, T_{cool} (130 °C) is lower from the viewpoint of the thermal recovery temperature (150 – 200 °C) of irradiated CuCrZr pipe. A comprehensive material database of Cu-alloy in T_{cool} (130 – 200 °C) range will be demanded for the divertor operation and determination of the replacement.

4.2.3. Thermal stress evaluation on high heat flux PFC

Elasto-plastic analysis with repeating high heat load is a common method to evaluate strain from the initial shape and thermal stress on the PFC component, which was performed for the JA-DEMO divertor target under the high peak q_{target} (10 and 15 MWm^{-2}) plus the nuclear heating condition [18], while non-irradiation stress–strain database was used. The maximum heat fluxes of 18 and 22 MWm^{-2}, respectively, are widely distributed on the water side of the CuCrZr pipe, which corresponded to 64% and 79% of CHF (28 MW m^{-2}) of the high T_{cool} (200 °C) coolant. For the latter case, the maximum temperature of the CuCrZr pipe was increased to ~380 °C. Expansions in the pipe axis (z) and circumferential (θ) directions are seen in the CuCrZr pipe under the MB tile, and compression is caused between MB tiles. While the stress (σ_Z) – strain (ε_Z) trace at the maximum stress location shows similar trajectory ($\Delta\sigma_Z$ ~ 300 MPa and $\Delta\varepsilon_Z$ ~ 0.25%) with repeated high heat load cycles. Mechanical toughness of the pipe against thermal softening may not be a critical lifetime issue at least for early stage of irradiated condition and the peak q_{target} of 15 MWm^{-2}, but it is anticipated to be critical with increasing the irradiation dose.

Uncertainty and/or limitations in lifetime projections of the CuCrZr pipe and Cu interlayer have been examined for the EU-DEMO divertor. Elasto-plastic analysis of the PFC component investigated under repeated high heat load of 20 MWm^{-2} level by using available neutron irradiation stress–strain database [69,70]. Even under non-irradiation condition, uncertainties come from (i) influences of initial residual stress on the cooling pipe and interlayer, (ii) shakedown response of the elasto-plastic structure in the early cycles, and (iii) loss of its initial yield strength by ageing (softening by thermal ageing) under the long-term cycles (in particular, exceeding the allowable service temperature limit of ~350 °C). For the neutron irradiation cases, the low T_{cool} (130 °C) would be still acceptable (suggested from ITER SDC-IC data) that the total elongation remained > 5% in embrittled CuCrZr pipe (for 0.3 – 5 dpa). Also it could be rather beneficial since the fracture toughness of the pipe (for 0.3 – 1 dpa) with a sub-mm level crack located at the inner wall is decreased with increasing temperature until no margin at ~350 °C for a large crack case. Furthermore, elasto-plastic analysis results suggest that the most likely failure behavior would be accumulated cyclic strain on the CuCrZr pipe surface, in particular, in the gap between adjacent W-MBs, leading to early fatigue cracks and potential coolant leaks. Consequently, elasto-plastic analysis study of the PFC unit (in particular, CuCrZr pipe) under the EU-DEMO divertor operation condition, i.e. the low T_{cool} and slow transient heat load of 20 MWm^{-2} level, has been developed under the above irradiation condition. Evaluation of the lifetime projection is in progress.

Copper interlayer could be hardened and embrittled when transmutation gas bubbles (e.g. helium) are segregated at grain boundaries at higher dose (~6 dpa). Embrittlement of the Cu interlayer leads to substantially high stresses (tensile stress on the W-MB), which may cause a crack formation of the W-MB at or near the bond interface, leading to a local reduction of heat conduction. Distinct consequences of limited knowledge on the actual state of materials and effective loading history are discussed in the light of expected failure modes. Degradation of the mechanical property of the heat sink and joint/interlayer caused by radiation induced softening and/or hardening at the lower dpa can be minimized by application of new W and Cu/Cu-alloy target concepts as shown in Sec. 4.3.

4.2.4. Cassette body and coolant design for DEMO divertors

CB design has been developed for each DEMO divertor to incorporate the power exhaust units and coolant pipes, which should be consistent with reducing the fast neutron flux to protect the vacuum vessel (less than 2.75 dpa for both JA- and EU-DEMO divertors) and replacement of the PFC units [18]. The number of main coolant pipes is minimized to four, and the inlet and outlet are located at the outboard cassette. The cassette structures and coolant conditions are different, but the CB can be made by welding similar RAFM-steel (F82H and Eurofer97).

The JA divertor CB consists of thick (25 cm) plate structures with two lines of cylindrical coolant puddles in order to reduce the fast neutron and γ-ray flux as shown in Fig. 14 (a). The exhaust slot is located at the outboard bottom in order to reduce the neutron flux to the vacuum vessel. The PWR condition coolant (290 °C, 15 MPa) is provided from the inboard and outboard manifolds through the side routes of the CB to the puddles, and it finally exits to a manifold near the exhaust slot. The coolant velocity of 1.5 m·s^{-1} is enough to remove the total nuclear heat of 0.7 MW in one cassette body, corresponding to a total of 32 MW for 48 cassettes.

The EU divertor CB is composed of a box structure with internal ribs, and it is cooled by higher inlet T_{cool} (180 °C, 3.5 MPa) coolant as shown in Fig. 15 (b) and (c), which ensures the entire structure sufficient fracture toughness at the neutron damage (less than 6 dpa) [54]. The coolant is also used for the liner and reflectors by a series connection. Since the exhaust opening is designed to be at the bottom of the CB, the liner mainly has a role in reducing fast neutron flux to the bottom area of the vacuum vessel. Total nuclear heat for 48 cassettes is 85 MW, which also includes the liner, reflectors and support structures of the target PFC units. In addition, that of 37 MW for the coolant fluid will be considered to evaluate T_{cool} in the circulation route.

The reduction in T_{cool} for the CB and RAFM heat sink of the PFC units is also a trade-off issue between irradiation embrittlement of the RAFM-steel and heat exhaust design. The low T_{cool} for the EU DEMO is

determined by the temperature margin (up to 550 °C) of key components such as supports of the reflector and liner plates due to inefficient exhaust of local nuclear heat. For the JA-DEMO divertor CB, local temperatures at the support structures of the inner and outer baffles are higher than 600 °C. Improvement of the heat exhaust design and the T_{cool} optimization are required.

4.3. Development of divertor target technologies for DEMO

The mechanical properties of the heat sink, the thermal contact to interlayer and the W-MB are important key issues for Cu-alloy application under neutron irradiation. Several technologies for the high heat flux target have been developed in the EU to survive under DEMO-relevant neutron irradiation conditions. All are based on W-MB as a baseline plasma facing material, and Cu-alloy pipe with swirl tape to increase the heat transfer at the pipe wall [71,72]. Material properties of CuCrZr and Cu-interlayer are anticipated to limit the performance of the target heat sink, e.g. irradiation creep above 350 °C and irradiation embrittlement below 250 °C [66]. Thus, the pipe is reinforced by various kinds of Cu-W composite materials and novel interlayer materials as shown in Fig. 17 [54].

(a) The ITER-like W-MB with a CuCrZr pipe [71,73] is a baseline concept also in the DEMO divertor, but the MB size is modified to decrease the cross-section width to 23 mm, instead of 28 mm in ITER in order to reduce thermal stresses and prevent vertical cracking. The axial block thickness of 12 mm and front face armor thickness of 8 mm above the cooling pipe are the baseline design.
(b) The thermal break interlayer concept (developed in Culham Centre for Fusion Energy: CCFE) is based on the ITER W-MB target [74]. The concept features cut-outs in the Cu-interlayer in the area of the highest heat flux to achieve a more uniform distribution of the thermal flux around the cooling pipe circumference.
(c) The composite pipe concept (developed in Max Planck Institute for Plasma Physics: IPP Garching) is based on a W wire-reinforced Cu composite pipe [75], which expects better strength of the cooling pipe, in particular, at high temperature (>350 °C).
(d) The functionally graded W/Cu (FGM) interlayer concept (developed in the French Alternative Energies and Atomic Energy Commission: CEA) aims to replace the thick Cu interlayer [76], which is expected to be fully embrittled by fast neutron due to segregation of transmuted He at grain boundaries. Graded thin (20 μm) and thick (500 μm) W-Cu interlayer is used to improve joining strength.
(e) The flat-tile concept with a composite heat sink block (developed in Max Planck Institute for Plasma Physics: IPP Garching) uses W-particle-reinforced Cu composite block [77,78] and it is expected to enhance the mechanical resilience of the irradiated heat sink against structure failure. The use of the W-Cu composite is supposed to reduce the thermal expansion mismatch between the armor tile and the heat sink block.
(f) In addition, He cooling of the target using multi-jet pipe by W and W-laminate (developed in Karlsruhe Institute of Technology: KIT) is also developed as a long-term option [71].

Recently, small-scale mock-ups of each concept have been fabricated and tested by means of hydrogen neutral beam in the GLADIS irradiation facility in IPP Garching under the high power density at 20 MWm^{-2} up to 2000 cycles (130 °C coolant, which is the expected operation temperature). A good production quality and reliable high-heat-flux fatigue performance was demonstrated. All mock-ups showed intact structural integrity and stable heat removal capacity over the entire loading cycles. Modest roughening of the W-MB surface and swelling of the blocks due to inelastic deformation was found. The metallographic examination revealed that the upper half of the MBs were completely recrystallized, but no discernable cracks were found in any of the tested armor (290 blocks). Furthermore, other ITER-like mock-ups were tested at 25 MWm^{-2} up to 1000 pulses (20 °C and 105 °C coolant conditions) for overload tests [79]. Also under the increased heat load, the mock-ups exhibited intact structural integrity and stable heat removal capacity, even though there was a single fine crack (6 mm in depth) initiated from the MB surface which underwent a pronounced inelastic deformation leading to overall severe roughening. The mock-ups even withstood the overload up to 32 MWm^{-2} (5 pulses), which was the physical limit nearly reaching the melting temperature of the W-MB surface without any detrimental impact nor melting. The future R&D will be focused on an upscaling trial towards a medium-scale manufacturing prototype (40 cm length).

Since oxide dispersion strengthened copper alloy (ODS-Cu) is also a suitable heat sink under the higher temperature and neutron irradiation condition as shown in Table 6, an advanced brazing technique (ABT) has been developed in Japan (National Institute for Fusion Science: NIFS) to join oxide dispersion strengthened copper alloy (ODS-Cu, i.e. such as Cu-0.3 wt%Al2O3: GlidCop®) heat sink and W-armor tile with the BNi-6 (Ni-11%P) filler material [80]. Recently, advanced multi-step brazing (AMSB) technique was applied to join ODS-Cu, W, and SUS with ODS-Cu

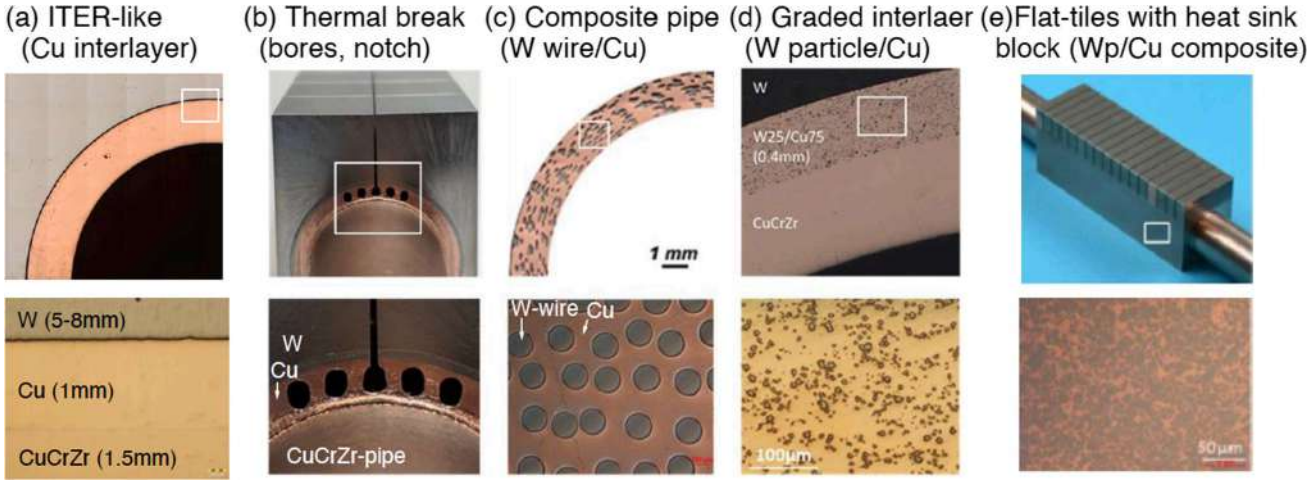

Fig. 17. High heat flux target technologies developed for EU-DEMO divertor [54]: (a) ITER-like monoblock baseline concept, (b) thermal break interlayer concept, (c) composite pipe of W-wire in Cu (Wf/Cu), (d) graded interlayer, (e) Flat W-tiles and W particle/Cu composite block. Bottom row of images show close up of region inside white rectangle above.

[81], so that prototype components for the divertor heat removal unit were successfully fabricated [63,82]. The component has a rectangle-shaped coolant flow path with V-shaped staggered rib (fin) structures in the flow path. High heat load tests by the electron beam device (ACT2 in NIFS) showed excellent heat removal capability up to 30 MWm^{-2} (15 °C, ~0.5 MPa water condition), using some heat removal enhancement such as turbulent flow and fine-scale local nucleate boiling. Optimization of the flat W-tile component and application to W-MB unit are planned for the future R&D.

5. Summary and future issues

The power exhaust concept and appropriate divertor design are common critical issues for DEMO design activities, which have been carried out in Europe, Japan, China, Korea and the USA. At the same time, the divertor design is strongly affected by DEMO missions (net electricity generation, sufficient tritium breeding and feasibility for remote maintenance) and the design requirements from each DEMO concept. In this paper, conventional divertor concepts and steady-state power exhaust studies for recent representative DEMO designs (P_{fusion} = 1 – 2 GW, R_p = 7 – 9 m) were reviewed from the viewpoints of the plasma physics issures and the engineering design. Radiative cooling is a common approach for the power exhaust scenario, and water-cooled divertor design with ITER-like target (W-PFC and Cu-alloy heat sink) is a common baseline. Common views and differences in the divertor designs are summarized below, and critical issues and challenges are clarified. Some different design approaches have provided important case-studies of the DEMO divertor, and those will contribute to future improvements and developments of the DEMO divertor design.

(1). Requirements of plasma performance and constraints on f_{rad}^{main} determine the divertor design concept:

Different power exhaust scenarios have been developed for DEMO concepts, while a common critical issue is the large power exhaust required to accomodate for P_{heat} = 280 – 600 MW. This demmands strong mitigation in the main plasma and divertor by the radiative cooling ($P_{rad}^{tot}/P_{heat} \geq 0.8$). The steady-state plasma concepts such as in JA-DEMO and CFETR proposed a conventional closed divertor geometry to challenge even large P_{sep}/R_p handling (25 – 30 MWm^{-1}) in order to maintain the ITER-level radiation fraction of the main plasma ($f_{rad}^{main} = P_{rad}^{main}/P_{heat}$ = 0.3 – 0.4) and higher plasma performance (HH_{98y2} = 1.2 – 1.4). K-DEMO and FNSF will challenge larger P_{sep}/R_p handling (37 – 53 MWm^{-1}) with the double-null divertor configuration. The repeating long pulsed plasma concept (EU-DEMO) challenges both increasing f_{rad}^{main} to ~0.65 with the ITER-level plasma performance (HH_{98y2} = 1.0 – 1.1) and handling the ITER-level P_{sep}/R_p in an open divertor geometry. The reactor plasma parameters B_T and R_p as well as exhaust power (P_{sep}) for the EU-DEMO were rather restricted by requirements of the divertor design for handling transient heat load due to divertor re-attachment, excessive impurity concentration to achieve the divertor detachment, and P_{sep} larger than P_{LH}. Optimization of competing requirements, i.e. increasing f_{rad}^{main} vs. the plasma performance ($HH_{98(y,2)}$, β_N, f_{BS}), is a common critical issue for these design concepts, and future experimental and modelling database will improve the power handling requirement for the divertor.

In addition, adequate performance of the power exhaust will be required in relatively low density plasmas. Design improvement is required from the viewpoints of reduction in the fuel dilution, and the power exhaust in the main plasma and divertor.

(2). Power exhaust simulations for DEMO divertor design (P_{sep} = 150 – 300 MW) are in progress and key issues for the plasma modelling of the partial detachment are recognized:

ITER-based divertor geometry (inclined target, baffle and dome structures) with longer leg length (1.6 – 1.7 m) is a common baseline design, and power exhaust simulations for DEMO divertor design with larger P_{sep} = 150 – 300 MW have been performed using integrated divertor codes; SOLPS-ITER on EU-DEMO and CFETR divertors, SONIC on JA-DEMO divertor, UEDGE on FNSF and K-DEMO divertors. Divertor operation and influences of the key power exhaust parameters have been recently investigated with mainly Ar seeding, and all simulations showed reduction in the peak $q_{target} \leq 10 MWm^{-2}$ for the divertor radiation fraction ($f_{rad}^{*div} = (P_{rad}^{div} + P_{rad}^{div})/P_{sep}$) of 0.7 – 0.8. Some results were consistent with the design requirement for the n_e^{sep} range (JA-DEMO: 2 – 3×10^{19}, EU-DEMO: ~3×10^{19} m^{-3}), which were relatively lower than that of ITER. All results also showed that partial detachment was expected in the outer divertor for the vertical target geometry, and the benefit of the closed geometry to reduce the peak q_{target} and T_e^{div} near the separatrix. A commonly recognized critical issue for the detachment simulations is that the peak q_{target} location and value (and each heat load components) significantly changed in the attached or detached region. In addition, uncertainty of relatively high T_e^{div} and T_i^{div} in the attached region (far-SOL) was another critical issue for plasma/impurity transport and tungsten (W) erosion. Further improvements of the divertor geometry and operation options such as different or mixed seeding impurities will be explored to extend the detachment radial width on the target and to reduce local T_e^{div} and T_i^{div} in the attached plasma region.

Radial diffusion coefficients of heat and particle fluxes (χ and D) are critical parameters for DEMO divertor design and operation. Different values and/or profiles were so far applied to produce $\lambda_{q//}$ =2 – 3 mm near the separatrix in the SOL, which was slightly smaller than that of ITER due to high T_e and T_i under the SOL condition of tokamak DEMO. Reduction in the assumed χ and D significantly affected the divertor power exhaust due to increase of the $q_{//i}$ profile in the SOL while the $q_{//e}$ profile was peaked near the separatrix. The transition location of near-SOL and far-SOL in the heat flux ($q_{//e} + q_{//i}$) profile approached to the separatrix. The transition location also corresponded to the flux surface of the detach-attach boundary at the outer target, and the peak q_{target} was increased with reducing the width of the partial detachment. Feasible values or profiles of the diffusion coefficients over the near- and far-SOLs will be required in order to determine the divertor operation for the DEMO design.

SOLPS-ITER simulation results with various drifts activated showed that, for these designs with ion ∇B drift towards the divertor, inboard-enhanced asymmetry of the particle flux profile and outboard-enhanced heat load profile were produced even in the long-leg divertors of EU-DEMO and CFETR. The latter recently proposed to further extend the divertor leg in order to insure the detached divertor operation window at lower n_e^{sep}. Other physics factors that could modify the DEMO divertor design such as enhanced power dissipations in the high density divertor (charge exchange, photon absorption and collisional-radiative models) and kinetic effects in the low collisionality SOL (flux limiter, thermal force) were also pointed out. It is an important common issue to clarify effects of these physics factors for the DEMO divertor conceptual design.

(3). The common baseline design for DEMO divertor and specific design were reviewed, and R&D issues were identified:

Integrated designs of the water cooled divertor target, cassette and coolant pipe routing have been developed, based on the ITER W monoblock (MB) concept with Cu-alloy pipe. Engineering design compatible with the higher DEMO-level neutron irradiation environment is required. Selection and arrangement of the divertor plasma facing unit, coolant condition and routing for recent design concepts of EU-DEMO, JA-DEMO, CFETR and K-DEMO were summarized. Under a year-long DEMO-level neutron irradiation condition, the mechanical properties of the CuCrZr heat sink and the Cu interlayer were anticipated to be embrittled, thus the coolant temperature (T_{cool}) for the high heat flux component was increased to higher than that of ITER (~70 °C). The inlet-T_{cool} selected so far showed a large variation between 70 °C and 200 °C (K-DEMO: 70 °C, EU-DEMO: 130 °C, CFETR: 140 – 180 °C, JA-DEMO: 200 °C). At the same time, the influence of thermal softening

on the CuCrZr pipe was evolved near the strike-point when the high heat load of 10 MWm^{-2}-level was applied, in particular, for the higher T_{cool} cases. DEMO specific risks such as neutron induced embrittlement/softening of the interlayers and cooling pipe have been recognized and further restrictions of q_{target} and surface temperature were anticipated. Elast-plastic analysis of the PFC unit under the EU-DEMO divertor operation condition, i.e. lower T_{cool} and slow transient heat load of 20 MWm^{-2} level, has been developed by using available irradiation database. Evaluation of the lifetime projection is in progress. Improved technologies of high heat flux components based on the ITER W-MB unit have been developed in the EU to reduce thermal stress and to strengthen the heat sink and interlayer under higher irradiation dose conditions.

Recent integrated design of the divertor target, CB and coolant pipe routing were also reviewed briefly. Two coolant conditions (low- and high-T_{cool}) were used for the Cu-alloy and RAFM-steel heat sink MB units, respectively, where the latter coolant was also used for the CB and supporting structures. Appropriate conditions for the latter coolant, i.e. 180 – 200 °C/ 5 MPa (EU-DEMO) and 290 °C/15 MPa (JA-DEMO, CFETR and K-DEMO), will be finalized in future optimizations of the divertor and DEMO design concept. Consequently, two coolant conditions and optimization of their circuits will be necessary for the water cooled DEMO divertor. The circuit design also should be appropriate for the remote maintenance and PFC replacement in the hot cell facility. In addition, a common issue of series or parallel cooling circuit routing for the DEMO divertor design was compared. The parallel circuit design for the target high heat flux PFCs becomes a common design for the EU- and JA-DEMO divertors in order to provide similar flow velocity of 10 $m{\cdot}s^{-1}$ to the inner and outer targets, while the series circuit is used for the ITER divertor.

CRediT authorship contribution statement

N. Asakura: Conceptualization, Methodology, Formal analysis, Investigation, Writing – original draft. **K. Hoshino:** Software, Methodology, Validation, Writing – review & editing. **S. Kakudate:** Investigation. **F. Subba:** Data curation, Validation, Writing – review & editing. **J.-H. You:** Data curation, Validation, Writing – review & editing. **S. Wiesen:** Validation. **T.D. Rognlien:** Data curation, Validation, Writing – review & editing. **R. Ding:** Data curation, Validation. **S. Kwon:** Data curation, Validation, Writing – review & editing.

Declaration of Competing Interest

The authors declare that they have no known competing financial interests or personal relationships that could have appeared to influence the work reported in this paper.

Data availability

Data will be made available on request.

Acknowledgments

The authors thank Y. Homma (QST), H. Utoh (QST), Y. Somaya (QST), S. Yamoto (QST), Y. Sakamoto (QST) , M. Tokitani (NIFS), Joint Special Design Team for Fusion DEMO (Japan), M. Siccinio (IPP, Garching), G. Mazzone (ENEA), D. Marzullo (Univ. Trieste), S. Roccella (ENEA), H. Greuner (MPG), C. Kessel (ORNL), S.-H. Hong (GA) for giving detailed information and comments. The first author also thanks the continuous support by the Japan and Europe home teams (QST in Rokkasho, and EUROfusion Programme Management Unit in Garching), and DEMO Design Activity (DDA) unit of the IFERC project team.

The SONIC simulations were carried out within the framework of the Broader Approach DEMO Design Activity, using the JFRS-1 supercomputer system at CSC, IFERC, Rokkasho, Japan.

References

[1] R. Wenninger, et al., The physics and technology basis entering European system code studies for DEMO, Nucl. Fusion 57 (2017), 016011.
[2] G. Federici, C. Bachmann, L. Barucca, W. Biel, L. Boccaccini, R. Brown, C. Bustreo, S. Ciattaglia, F. Cismondi, M. Coleman, V. Corato, C. Day, E. Diegele, U. Fischer, T. Franke, C. Gliss, A. Ibarra, R. Kembleton, A. Loving, F. Maviglia, B. Meszaros, G. Pintsuk, N. Taylor, M.Q. Tran, C. Vorpahl, R. Wenninger, J.H. You, DEMO design activity in Europe: progress and updates, Fusion Eng. Des. 136 (2018) 729–741.
[3] G. Federici, et al., Overview of the DEMO staged design approach in Europe, Nucl. Fusion 59 (2019), 066013.
[4] Y. Sakamoto, et al., DEMO Concept Development and Assessment of Relevant Technologies, 25th IAEA Int. Conf. on Fusion Energy (St. Petersburg, Russia, 2014) FIP/3-2Rb.
[5] K. Tobita, et al., Design strategy and recent design activity on Japan's DEMO, Fusion Sci. Technol. 72 (2017) 537.
[6] N. Asakura, et al., Studies of power exhaust and divertor design for a 1.5 GW-level fusion power DEMO, Nucl. Fusion 57 (2017), 126050.
[7] G. Zhuang, G.Q. Li, J. Li, Y.X. Wan, Y. Liu, X.L. Wang, Y.T. Song, V. Chan, Q. W. Yang, B.N. Wan, X.R. Duan, P. Fu, B.J. Xiao, Progress of the CFETR design, Nucl. Fusion 59 (11) (2019) 112010.
[8] K. Kim, et al., Design of K-DEMO for near-term implementation, Nucl. Fusion 55 (2015), 053027.
[9] J.S. Kang, et al., Development of a systematic, self-consistent algorithm for the K-DEMO steady-state operation scenario, Nucl. Fusion 57 (2017), 126034.
[10] C.E. Kessel, D.B. Batchelor, P.T. Bonoli, M.E. Rensink, T.D. Rognlien, P. Snyder, G. M. Wallace, S.J. Wukitch, Core plasma physics basis and its impacts on the FNSF, Fusion Eng. Des. 135 (2018) 356–369.
[11] C.E. Kessel, et al., The ARIES advanced and conservative tokamak power plant study, Fusion Sci. Technol. 67 (2015) 1.
[12] M. Shimada, D.J. Campbell, V. Mukhovatov, M. Fujiwara, N. Kirneva, K. Lackner, M. Nagami, V.D. Pustovitov, N. Uckan, J. Wesley, N. Asakura, A.E. Costley, A.J. H. Donné, E.J. Doyle, A. Fasoli, C. Gormezano, Y. Gribov, O. Gruber, T.C. Hender, W. Houlberg, S. Ide, Y. Kamada, A. Leonard, B. Lipschultz, A. Loarte, K. Miyamoto, V. Mukhovatov, T.H. Osborne, A. Polevoi, A.C.C. Sips, Chapter 1: overview and summary, Nucl. Fusion 47 (6) (2007) S1–S17.
[13] A. Loarte, B. Lipschultz, A.S. Kukushkin, G.F. Matthews, P.C. Stangeby, N. Asakura, G.F. Counsell, G. Federici, A. Kallenbach, K. Krieger, A. Mahdavi, V. Philipps, D. Reiter, J. Roth, J. Strachan, D. Whyte, R. Doerner, T. Eich, W. Fundamenski, A. Herrmann, M. Fenstermacher, P. Ghendrih, M. Groth, A. Kirschner, S. Konoshima, B. LaBombard, P. Lang, A.W. Leonard, P. Monier-Garbet, R. Neu, H. Pacher, B. Pegourie, R.A. Pitts, S. Takamura, J. Terry, E. Tsitrone, T.-O. Group, Chapter 4: power and particle control, Nucl. Fusion 47 (6) (2007) S203–S263.
[14] N. Asakura, et al., Simulation studies of divertor detachment and critical power exhaust parameters for Japanese DEMO design, Nucl. Meter. Energy 26 (2021), 100864.
[15] N. Asakura, et al., Development and application of SONIC divertor simulation code to power exhaust design of Japanese DEMO divertor, Processes 10 (2022) 872.
[16] F. Subba, et al., Modelling of mitigation of the power divertor loading for the EU DEMO through Ar injection, Plasma Phys. Control. Fusion 60 (2018), 035013.
[17] F. Subba, et al., SOLPS-ITER modeling of divertor scenarios for EU-DEMO, Nucl. Fusion 61 (2021), 106013.
[18] N. Asakura, et al., Power exhaust concepts and divertor designs for japanese and european DEMO fusion reactors, Nucl. Fusion 61 (2021), 126057.
[19] L. Aho-Mantila, et al., Predictions of radiation pattern and in–out asymmetries in the DEMO scrape-off layer using fluid neutrals, Nucl. Fusion 62 (2022), 056015.
[20] X.J. Liu, et al., Simulation studies of divertor power exhaust with neon seeding for CFETR with GW-level fusion power, Phys. Plasmas 27 (2020), 092508.
[21] H. Si, et al., SOLPS-ITER simulations of high power exhaust for CFETR divertor with full drifts, Nucl. Fusion 62 (2022), 026031.
[22] S. Kwon, K. Im, S.-H. Hong, H. Lee, T.D. Rognlien, W. Meyer, K. Kim, Recent progress in the design of the K-DEMO divertor, Fusion Eng. Des. 159 (2020) 111770.
[23] T.D. Rognlien, M.E. Rensink, D.P. Stotler, Scrape-off layer plasma and neutral characteristics and their interactions with walls for FNSF, Fusion Eng. Des. 135 (2018) 380–393.
[24] M.E. Rensink, T.D. Rognlien, Plasma heat-flux dispersal for ACT1 divertor configurations, Fusion Sci. Technol. 67 (1) (2015) 125–141.
[25] R.A. Pitts, et al., Physics basis for the first ITER tungsten divertor, Nucl. Meter. Energy 20 (2019), 100696.
[26] R.A. Pitts, S. Carpentier, F. Escourbiac, T. Hirai, V. Komarov, S. Lisgo, A. S. Kukushkin, A. Loarte, M. Merola, A. Sashala Naik, R. Mitteau, M. Sugihara, B. Bazylev, P.C. Stangeby, A full tungsten divertor for ITER: physics issues and design status, J. Nucl. Mater. 438 (2013) S48–S56.
[27] N. Asakura, Recent Developments of Plasma Exhaust and Divertor Design for Tokamak DEMO Reactors, 25th International Conference on Plasma Surface Interactions in Controlled Fusion Devices (remote, Korea, 13–17 June 2022) MR01.
[28] M. Siccinio, et al., Figure of merit for divertor protection in the preliminary design of the EU-DEMO reactor, Nucl. Fusion 59 (2019), 106026.
[29] M. Kovari, et al., PROCESS: a systems code for fusion power plants-Part 2: engineering, Fusion Eng. Des. 104 (2016) 9.
[30] M. Nakamura, et al., Efforts towards improvement of systems codes for the Broader Approach DEMO design, Fusion Eng. Des. 87 (2012) 864.
[31] N. Asakura, et al., A simulation study of large power handling in the divertor for a Demo reactor, Nucl. Fusion 53 (2013), 123013.

[32] R. Wenninger, et al., Advances in the physics basis for the European DEMO design, Nucl. Fusion 55 (2015), 063003.
[33] Y.R. Martin, T. Takizuka, T.-M. Group, Power requirement for accessing the H-mode in ITER, J. Phys.: Conf. Ser. 123 (2008) 012033.
[34] A. Kallenbach, et al., Optimized tokamak power exhaust with double radiative feedback in ASDEX Upgrade, Nucl. Fusion 52 (2012), 122003.
[35] A. Kallenbach, et al., Partial detachment of high power discharges in ASDEX Upgrade, Nucl. Fusion 55 (2015), 053026.
[36] P. Pereslavtsev, et al., Neutronic analyses of generic issues affecting thetritium breeding performance in different DEMO blanket concepts, Fusion Eng. Des. 109–111 (2016) 1207–1211.
[37] N. Asakura, et al., Investigations of impurity seeding and radiation control for long-pulse and high-density H-mode plasmas in JT-60U, Nucl. Fusion 49 (2009), 115010.
[38] H. Utoh, et al., Studies of the plasma vertical instability and its control concepts in JA and EU broader approach, DEMO design activity, Fusion Eng. Des. 136 (2018) 874.
[39] A. Huber, et al., Comparative H-mode density limit studies in JET and AUG, Nucl. Metter. Energy 12 (2017) 100.
[40] A.S. Kukushkin, H.D. Pacher, G.W. Pacher, V. Kotov, R.A. Pitts, D. Reiter, Consequences of a reduction of the upstream power SOL width in ITER, J. Nucl. Mater. 438 (2013) S203–S207.
[41] T. Eich, et al., Scaling of the tokamak near the scrape-off layer H-mode power width and implications for ITER, Nucl. Fusion 53 (2013), 093031.
[42] A. Kallenbach, N. Asakura, A. Kirk, A. Korotkov, M.A. Mahdavi, D. Mossessian, G. D. Porter, Multi-machine comparisons of H-mode separatrix densities and edge profile behaviour in the ITPA SOL and Divertor Physics Topical Group, J. Nucl. Mater 337-339 (2005) 381–385.
[43] A.W. Leonard, et al., Compatibility of separatrix density scaling for divertor detachment with H-mode pedestal operation in DIII-D, Nucl. Fusion 57 (2017), 086033.
[44] T. Eich, et al., JET Contributors; Correlation of the tokamak H-mode density limit with ballooning stability at the separatrix, Nucl. Fusion 58 (2018), 034001.
[45] A. Loarte, Effects of divertor geometry on tokamak plasmas, Plasma Phys. Control. Fusion 43 (6) (2001) R183–R224.
[46] S. Qin, et al., Design analysis and remote handling compatibility for a CFETR long leg divertor concept, Fusion Eng. Des. 167 (2021), 112351.
[47] D. Reiter, The TRIM code surface database (http://eirene.de/trim.pdf) (2010).
[48] P.C. Stangeby, J.D. Elder, Calculation of observable quantities using a divertor impurity interpretive code DIVIMP, J. Nucl. Mater. 196–198 (1992) 258.
[49] P.C. Stangeby, The plasma boundary of magnetic fusion devices, IOP Publishing, 2000.
[50] A.V. Chankin, et al., Monte Carlo simulations of tungsten redeposition at the divertor target, Plasma Phys. Control. Fusion 56 (2014), 025003.
[51] F. Maviglia, G. Federici, G. Strohmayer, R. Wenninger, C. Bachmann, R. Albanese, R. Ambrosino, M. Li, V.P. Loschiavo, J.H. You, L. Zani, Limitations of transient power loads on DEMO and analysis of mitigation techniques, Fusion Eng. Des. 109-111 (2016) 1067–1071.
[52] S.I. Krasheninnikov, Reverse flow and parameter profiles in a dense tokamak divertor plasma, Nucl. Fusion 32 (1992) 1927–1934.
[53] G. Mazzone, J.-H. You, C. Bachmann, U. Bonavolontà, V. Cerri, D. Coccorese, D. Dongiovanni, D. Flammini, P. Frosi, L. Forest, G. Di Gironimo, G. Di Mambro, V. Imbriani, A. Maffucci, D. Marzullo, P.A. Di Maio, M.T. Porfiri, E. Vallone, R. Villari, E. Visca, C. Vorpahl, Eurofusion-DEMO divertor - cassette design and integration, Fusion Eng. Des. 157 (2020) 111656.
[54] J.H. You, et al., Divertor of the European DEMO: engineering and technologies for power exhaust, Fusion Eng. Des. 175 (2022), 113010.
[55] X.Y. Qian, et al., New designs of target and cooling scheme for water cooled divertor in DEMO, Nucl. Fusion 61 (2021), 036008.
[56] R. Villari, et al., Nuclear analysis of the ITER full-tungsten divertor, Fusion Eng. Des. 88 (2013) 2006.
[57] G. Federici, et al., Overview of the design approach and prioritization of R&D activitiestowards an EU DEMO, Fusion Eng. Des. 109–111 (2016) 1464–1474.
[58] H. Utoh, S. Kakudate, R. Hiwatari, Y. Someya, Y. Sakamoto, N. Asakura, S. Tokunaga, K. Tobita, Progress on reliability of remote maintenance concept for JA DEMO, Fusion Eng. Des. 146 (2019) 1583–1586.
[59] A. Hasegawa, et al., Neutron irradiation effects on tungsten materials, J. Nucl. Mater. 89 (2014) 1568–1572.
[60] Y. Ueda, et al., Baseline high heat flux and plasma facing materials for fusion, Nucl. Fusion 57 (2017), 092006.
[61] C.h. Linsmeier, et al., Development of advanced high heat flux and plasma-facing materials, Nucl. Fusion 57 (2017), 092007.
[62] A. Alfonso, et al., Thermal stability of a highly-deformed warm-rolled tungsten plate in the temperature range 1100–1250°C, Fus. Eng. Des. 98–99 (2015) 1924.
[63] M. Tokitani, et al., Fabrication of divertor mock-up with ODS-Cu and W by the improved brazing technique, Nucl. Fusion 57 (2017), 076009.
[64] S.A. Fabritsiev, S.J. Zinkle, B.N. Singh, Evaluation of copper alloys for fusion reactor divertor and first wall components, J. Nucl. Mater. 233-237 (1996) 127–137.
[65] S.A. Fabritsiev, A.S. Pokrovsky, Effect of high doses of neutron irradiation on physicomechanical properties of copper alloys for ITER applications, Fusion Eng. Des. 73 (1) (2005) 19–34.
[66] J.-H. You, et al., A review on two previous divertor target concepts for DEMO: mutual impact between structural design requirements and materials performance, Nucl. Fusion 55 (2015), 113026.
[67] Y. Someya, et al., Design study of blanket structure based on a water-cooled solid breeder for DEMO, Fusion Eng. Des. 98–99 (2015) 1872.
[68] S. Kwon, K. Im, J.S. Park, Thermo-hydraulic optimization study for a high heat flux unit of the K-DEMO divertor target, Fusion Eng. Des. 134 (2018) 68–73.
[69] M. Fursdon, J.-H. You, Towards reliable design-by-analysis for divertor plasma facing components—Guidelines for inelastic assessment (part II: irradiated), Fusion Eng. Des. 160 (2020) 111831.
[70] J.-H. You, M. Li, K. Zhang, Structural lifetime assessment for the DEMO divertor targets: design-by-analysis approach and outstanding issues, Fusion Eng. Des. 164 (2021) 112203.
[71] J.H. You, et al., European divertor target concepts for DEMO: design rationales and high heat flux performance, Nucl. Mater. Energy 16 (2018) 1.
[72] J.-H. You, et al., High-heat-flux technologies for the European demo divertor targets: State-of-the-art and a review of the latest testing campaign, J. Nucl. Mater. 544 (2021), 152670.
[73] F. Crescenzi, et al., Design study of ITER-like divertor target for DEMO, Fusion Eng. Des. 98–99 (2015) 1263.
[74] F. Domptail, et al., The design and optimisation of a monoblock divertor target for DEMO using thermal break interlayer, Fusion Eng. Des. 154 (2020), 111497.
[75] A.v. Müller, et al., Application of tungsten-copper composite heat sink materials to plasma-facing component mock-ups, Phys. Scr. T 171 (2020), 014015.
[76] M. Richou, et al., Performance assessment of thick W/Cu graded interlayer for DEMO divertor target, Fusion Eng. Des. 157 (2020), 111610.
[77] J.-H. You, A. Brendel, S. Nawka, T. Schubert, B. Kieback, Thermal and mechanical properties of infiltrated W/CuCrZr composite materials for functionally graded heat sink application, J. Nucl. Mater. 438 (1-3) (2013) 1–6.
[78] E. Tejado, A.v. Müller, J.-H. You, J.Y. Pastor, The thermo-mechanical behaviour of W-Cu metal matrix composites for fusion heat sink applications: the influence of the Cu content, J. Nucl. Mater. 498 (2018) 468–475.
[79] J.H. You, et al., High-heat-flux performance limit of the tungsten monoblock targets: Impact on armor materials and implications for power exhaust, Nucl. Mater. Energy accepted.
[80] M. Tokitani, Y. Hamaji, Y. Hiraoka, S. Masuzaki, H. Tamura, H. Noto, T. Tanaka, T. Muroga, A. Sagara, Deformation and fracture behavior of the W/ODS-Cu joint fabricated by the advanced brazing technique, Fusion Eng. Des. 146 (2019) 1733–1736.
[81] M. Tokitani, et al., Application of the advanced multi-step brazing for fabrication of the high heat flux component, J. Nucl. Mater. 538 (2020), 152264.
[82] M. Tokitania, et al., Advanced multi-step brazing for fabrication of a divertor heat removal component, Nucl. Fusion 61 (2021), 046016.